J. Fluid Mech. (1988), *vol.* 190, *pp.* 55–70
Printed in Great Britain

The growth of a turbulent patch in a stratified fluid

By HARINDRA J. S. FERNANDO
Department of Mechanical and Aerospace Engineering, Arizona State University, Tempe, AZ 85287, USA

(Received 16 April 1985 and in revised form 22 September 1987)

The behaviour of a turbulent region generated within a linearly-stratified fluid by an external energy source has been studied experimentally. A monoplanar grid that generated small-amplitude oscillations was used as the energy source. The results show that the mixed layer initially grows rapidly, as in an unstratified fluid, but when its physical vertical size becomes $r_f \sim (K_1/N)^{\frac{1}{2}}$, at a time $t_f \approx 4.0\,N^{-1}$, where N is the buoyancy frequency and K_1 is the 'action' of the grid, the buoyancy forces become dominant and drastically reduce further vertical growth of the patch. While the patch size remains at r_f, a well-defined density interfacial layer is formed at the entrainment interface. An important feature of the interfacial layer is the presence of internal waves, excited by the mixed-layer turbulence. If the grid oscillations are continuously maintained, the interfacial waves break and cause turbulent mixing, thereby increasing the size of the patch beyond r_f at a very slow rate. Theoretical estimates are made for the growth characteristics and are compared with the experimental results.

1. Introduction

Recent laboratory experiments (McEwan 1983*a*, *b*) and oceanic observations (Osborn 1980) provide strong evidence that turbulence in stratified media is confined to intermittently occurring turbulent patches, which are distributed randomly in otherwise laminar fluid. The reason for this behaviour, as pointed out by Dougherty (1961), Ozmidov (1965) and others, is the inability of a stratified turbulent region to grow beyond a certain vertical lengthscale, referred to as the limiting lengthscale. In stratified media, turbulent patches can usually be generated by instability mechanisms such as wave breaking and double diffusion.

Several evolutionary scenarios have been proposed for oceanic turbulent patches with each investigator taking a personal point of view. Gibson (1986), for example, maintains that almost all observed patches of turbulence in the ocean are fossil remnants from previously active patches, whereas others (e.g. Crawford 1982; Dillon 1982; Caldwell 1983) believe that ocean microstructure patches are active, with the largest eddies in the patches in equilibrium with the forcing shear flow. A few laboratory experiments and field observations have been reported on the nature of stratified turbulence, but none of these studies have dealt with the characteristics of a single turbulent patch. Evidently, without an understanding of the dynamics of the patches and their distribution in space and time, the interpretation of stratified turbulence experiments is difficult. As pointed out by Gibson (1981), measurements of average turbulent quantities of oceanic turbulence, with a dropsonde, give a single vertical cut through the stratified layer and the average of the sample may not be the average of the intermittently occurring patches. Similar situations also arise in

laboratory experiments. For example, when a stationary probe is used to measure stratified turbulence in the presence of a mean flow (e.g. Stillinger, Hellend & Van Atta 1983), the measured turbulent quantities may not be the same as those of a patch due to the intermittent occurrence of the patches. To overcome such ambiguities, it was decided to generate a turbulent patch in a linearly-stratified fluid by a known localized, shear-free energy source and to study its growth behaviour. Because the patch is not advected, detailed flow visualization and the measurement of its growth characteristics are possible, although, since there is no mean flow, accurate measurement of some quantities, such as the turbulent kinetic energy dissipation, is not practicable. One possibility would be to use a rotating or a shooting hot-film probe to simulate the mean flow, but the small size of the turbulent patches does not permit such an arrangement.

A planar oscillating grid that generated small-amplitude oscillations was selected as the turbulent energy source. There are two reasons for this choice. First, the nature of oscillating-grid turbulence has been widely studied, both experimentally (Hopfinger & Toly 1976) and theoretically (Long 1978*a*). These studies show that the horizontal (u, v) and vertical (w) r.m.s. velocity components and the integral lengthscale l of turbulence at a distance z away from the grid plane are given by

$$u \simeq v \sim w \propto \omega z^{-1}, \tag{1}$$

and

$$l \sim z, \tag{2}$$

such that $uz = K_1$, where K_1 is the 'action' parameter introduced by Long (1978*a*) as the sole parameter necessary to describe grid-induced turbulence at high Reynolds number. On dimensional grounds, $K_1 \propto \omega$, where ω is the frequency of the grid oscillations. Secondly, as postulated by Long (1986), the concept of 'action' is applicable to a wide variety of other zero-mean-shear energy sources, such as the turbulence generated by a uniform mean flow past a grid. On this premise, it is expected that the present experimental results will be helpful in interpreting, at least qualitatively, the observed features of some previous stratified-flow experiments.

In summary, the aim of the present work is to examine experimentally the growth of a turbulent region in a linearly-stratified fluid and to interpret the experimental observations in terms of the characteristics of the stratification and the turbulence.

2. Experimental procedure

Figure 1 shows a schematic view of the experimental apparatus. The experiments were conducted in a 26 cm × 26 cm × 30 cm Plexiglas tank with a 'capped hole' in the bottom face to supply stratifying salt water. The standard two-tank technique of Oster & Yamamato (1963) was used to obtain a linear stratification. At the mid-depth of the tank a metallic-mesh grid was suspended by a thin, rigid brass rod of 4 mm diameter. The grid was constructed by drilling 4 mm diameter holes, with a centre to centre distance of 5.6 cm in a 1.5 mm thick aluminium sheet so that the centres of the holes form a square mesh. The solidity of the grid is about 40%. The rod supporting the grid was connected to the slider of an oscillating mechanism designed to work on a slider-crank principle.

The mechanism was powered by a direct-current, high traction motor via a reduction gear box and a flywheel. The stroke S and frequency ω of the grid oscillations could be varied from 4 mm to 3 cm and up to 5 Hz, respectively. However, only a small frequency range could be achieved, due to impulsive loading

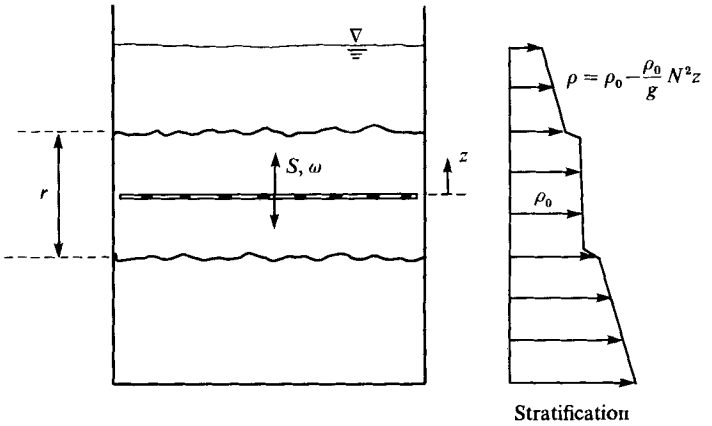

FIGURE 1. A schematic diagram showing the generation of a turbulent region within a linearly stratified fluid by an oscillating grid.

during start-up, and vibrational problems. In the experiments reported here, the lowest possible stroke for the grid oscillations (4 mm) has been used. The diameter of the rod connecting the grid and the oscillator was selected to ensure that there was no appreciable mixing due to the rod's vertical oscillations within the stratified region. The absence of such mixing was confirmed by shadowgraph observations. The density measurements were made with a two-electrode conductivity probe connected to a balanced a.c. bridge. The buoyancy frequency N was calculated by fitting a least square line to the data which related density ρ to depth z (figure 1) and using the expression $N^2 = -(g/\rho_0)(\mathrm{d}\rho/\mathrm{d}z)$, where g is the gravitational acceleration. The reference density ρ_0 was selected as the density corresponding to the mid-plane of the grid.

At the beginning of the experiments, the motor and the gear box were decoupled from the oscillating mechanism and the motor was allowed to run for several minutes to attain the correct steady operating conditions. The experiments were started by engaging the oscillating mechanism to the motor. Filming with a 16 mm movie camera (at 32 frames per second) was begun a little before the grid oscillations so that the time origin of the mixed-layer growth could be determined. The onset time of the grid oscillations was taken as the time origin. The filming continued until the mixed region had grown to a steady state. To cover a single experiment, several reels of film were necessary; growth information could not be obtained during the time of the film changeover. The position of the turbulent front could be easily identified by its image which formed on the shadowgraph as a result of refractive-index fluctuations. Some experiments were also performed using homogeneous fluids and the position of the turbulent front was then observed using suspended aluminium flakes, illuminated by a powerful light source, as in Dickinson & Long (1983).

To analyse the films, the reels were loaded in a computer-controlled movie analyser which had the capability to advance and analyse the film frame by frame. The image of the turbulent front was obtained on a digitizing pad and the x, z position of the front was recorded. The mean (averaged over x) vertical positions of the fronts above and below the grid were determined and the distance between them was considered to be the physical vertical size of the patch r. To avoid spurious data due to possible forced flow near the grid, the readings for the turbulent front position were taken

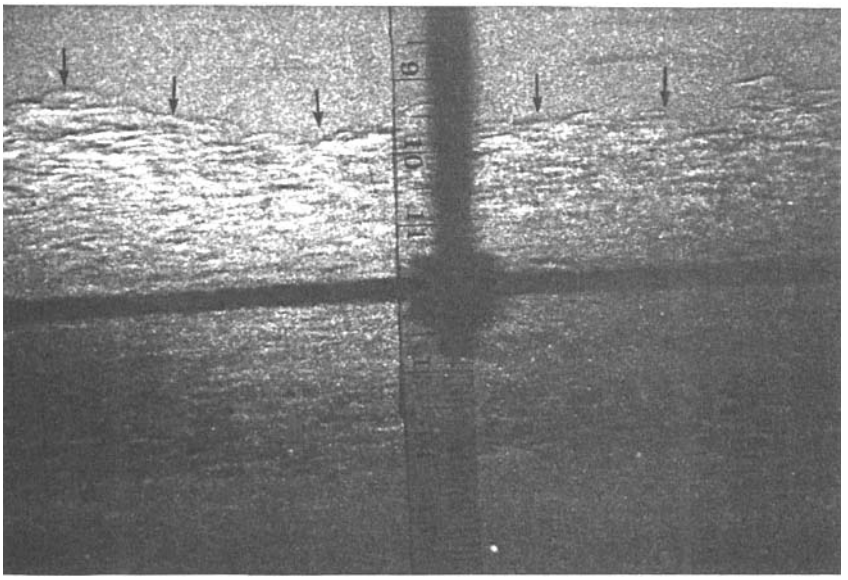

FIGURE 2. Growth of a grid-generated mixed region in a linearly stratified fluid at $t < t_f$. Notice the absence of a well-defined interfacial layer at the entrainment interface. The arrows show the turbulent front. This picture was taken at $Nt \simeq 2.5$.

after the mixed region had grown to a thickness of 1.5 cm, which is about 3.75 times the stroke of the grid oscillations. Once the mixed region had grown to a steady thickness, an interfacial layer was observed to form; this layer contained interfacial waves. The amplitude and frequency data of the waves were extracted from the film using the technique described in detail by Wyatt (1978), and the average wave heights and the frequencies were then calculated. The number of waves analysed for a given run was around 25–30.

3. Experimental observations

3.1. *Visualization of the flow*

By replaying the films taken during the experiments several times, the growth of the turbulent patch with time was carefully observed. When the grid started its oscillations, the turbulent layer that formed on either side of the grid grew rapidly until it reached the limiting (physical) patch size (subscript f corresponds to conditions at the limiting size) $r = r_f$ at a time $t = t_f$, where a drastic reduction of the propagation speed could be observed. At $t < t_f$ (henceforth referred to as the 'initial growth' regime), the front was found to be sharp and visible on a shadowgraph (figure 2). Neither a well-defined interfacial layer (a transition region between the mixed region and unperturbed fluid with finite density gradients) nor interfacial waves could be identified. The appearance of the front was wavy and contorted and was similar to that observed during the experiments performed in a homogeneous fluid (seeded with aluminium flakes for flow visualization). This is expected since, during the initial growth, the turbulent eddies are energetic enough to entrain as in a homogeneous fluid despite the buoyancy effects. At $t = t_f$, the entrainment virtually stops, the patch size assumes a quasi-steady value, and an interfacial layer

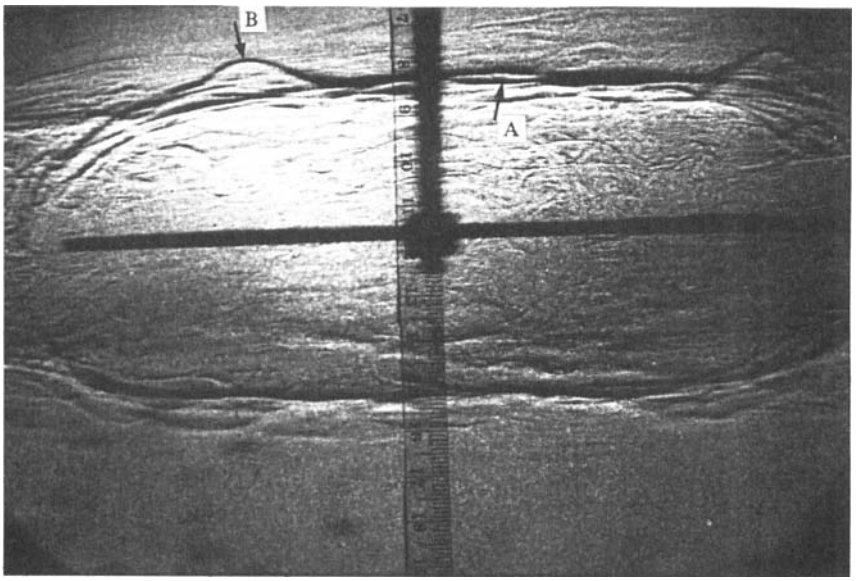

FIGURE 3. Appearance of the turbulent patch at $t \geqslant t_f$. Note the presence of a well-defined interfacial layer (A) and the interfacial waves (B). This picture was taken at $Nt \simeq 20$.

gradually appears to form at the turbulent–non-turbulent front (figure 3). Simultaneously, internal waves, that are excited by the mixed-layer turbulence, could also be seen. If the grid oscillations were continuously maintained for times $t \gg t_f$, the interfacial waves were found to break, thus causing turbulent mixing, and the mixed region was found to grow beyond the size r_f at a very slow rate. This growth beyond r_f ($t \gg t_f$) will be referred to as 'subsequent growth'.

3.2. *The growth characteristics of the turbulent patch*

On dimensional grounds, for high-Reynolds-number turbulence, the vertical size of the patch r at any time t can be written as

$$r = f(K_1, N, t), \tag{3a}$$

or

$$r/(K_1/N)^{\frac{1}{2}} = f_1(Nt), \tag{3b}$$

where f and f_1 are functionals. As mentioned in §2, measurements of the vertical growth of the patch have been made; the results are presented in figure 4 as a plot of $r/(\omega/N)^{\frac{1}{2}}$ *vs.* Nt. The scaling parameter for the length $(\omega/N)^{\frac{1}{2}}$ was selected because of the condition $K_1 \propto \omega$. The measurements clearly show that the growth rate of the patch is drastically reduced, quite abruptly, at a non-dimensional time $Nt_f \approx 4.0$, when the patch has grown to a thickness $r_f \simeq 1.47(\omega/N)^{\frac{1}{2}}$. The solid line drawn up to $Nt = 4.0$ in figure 4 represents the theoretical estimate made in §4.1 for the growth at times $t < t_f$. As will be discussed in §4.1, the initial growth is similar to the growth behaviour observed in homogeneous fluids, indicating that, prior to the mixed region growing to the size r_f, the buoyancy forces have an insignificant effect on the mixed-layer growth.

Detailed experiments were performed to investigate the dependency of the limiting patch thickness r_f on K_1 (or ω) and N; the results are presented in figures 5–7. Figure 5 shows the variation of the half limiting patch thickness with N, for the

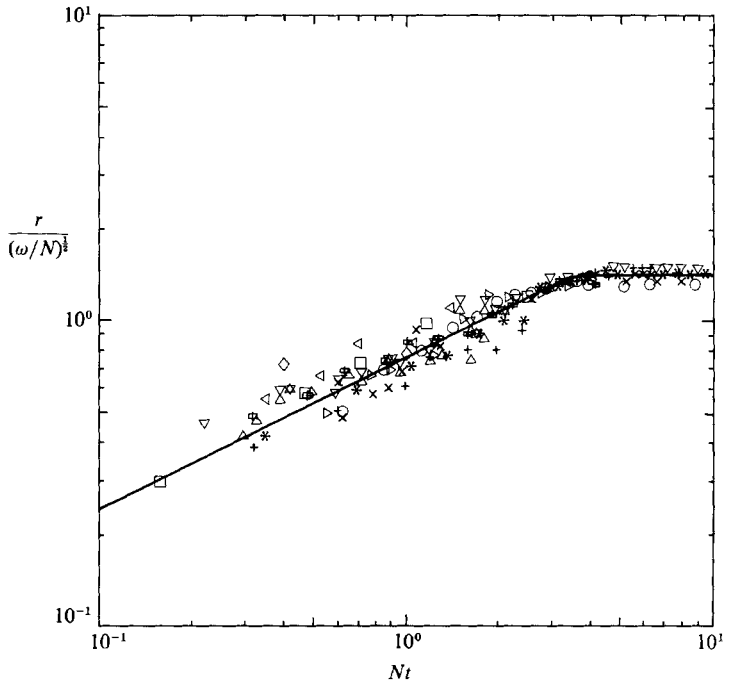

FIGURE 4. Initial growth of the turbulent patch. Variation of $r/(\omega/N)^{\frac{1}{2}}$ [which is proportional to $r/(K_1/N)^{\frac{1}{2}}$] with Nt. Solid line up to the limiting thickness r_f is drawn according to (10). r is in cm, ω and N are in rad/s. Symbols represent ∇, $N = 0.700$, $\omega = 12.75$; ○, 0.904, 13.24; ×, 0.972, 13.14; ▷, 0.996, 12.75; □, 1.020, 13.14; ×, 1.042, 13.42; △, 1.045, 12.79; *, 1.104, 12.15; ◇, 1.108, 12.75; ◁, 1.110, 12.79; ▽, 1.115, 12.79; ⊞, 1.252, 12.79; +, 1.274, 12.79; ✡, 1.343, 13.14.

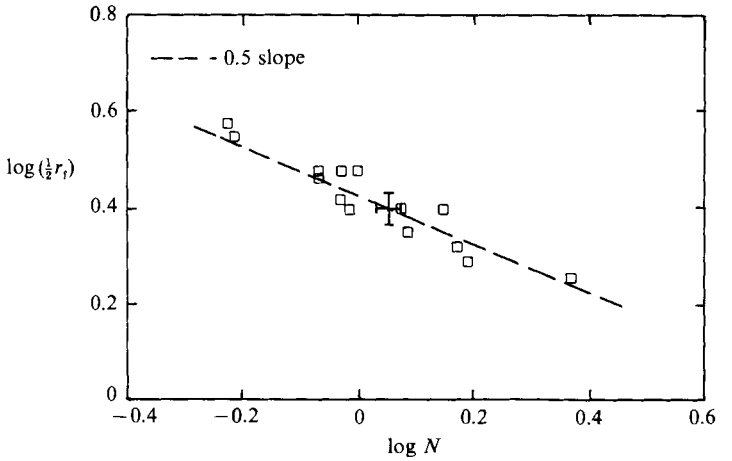

FIGURE 5. Variation of $\log(\frac{1}{2}r_f)$ with $\log N$ at constant $\omega \simeq 12.5$ rad/s^{-1} (or constant K_1). r_f is in cm and N is in rad/s.

experiments performed at constant ω. Over the range of N investigated, 0.4 to 2.25 s^{-1}, the results follow the power law relationship $r_f \propto N^{-\frac{1}{2}}$. As shown in figure 6, the experiments performed at constant N suggest $r_f \propto \omega^{\frac{1}{2}} \propto K_1^{\frac{1}{2}}$, for the range $\omega = 9.5$–16.5 s^{-1}. Figure 7 shows the variation of the limiting patch thickness with the lengthscale $(K_1/N)^{\frac{1}{2}} \propto (\omega/N)^{\frac{1}{2}}$. During the experiments, the Reynolds number K_1/ν,

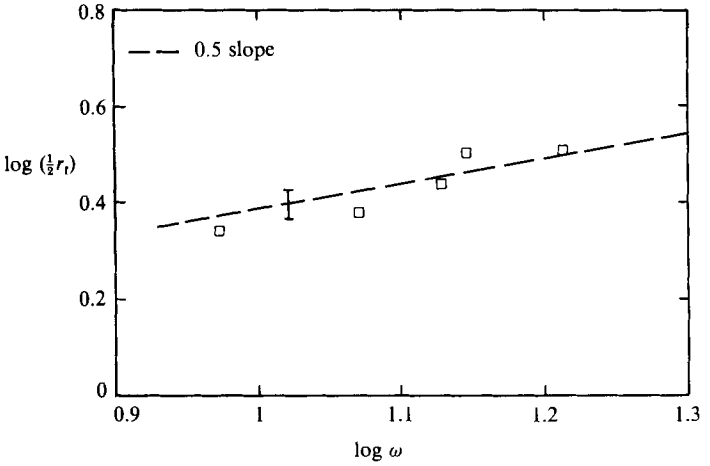

FIGURE 6. Variation of log ($\frac{1}{2}r_f$) with log ω at constant $N = 1.05$. r_f is in cm and ω and N are in rad/s.

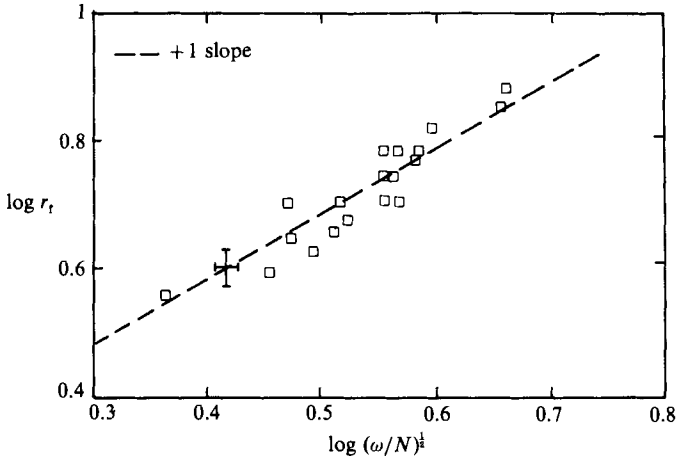

FIGURE 7. Variation of log r_f with log $(\omega/N)^{\frac{1}{2}}$ [which is proportional to log $(K_1/N)^{\frac{1}{2}}$]. r_f is in cm, ω and N are in rad/s.

where ν is the kinematic viscosity, was varied by a factor of 1.8, but no systematic dependence of r_f on the Reynolds number could be observed.

3.3 *Measurements of the interfacial wave characteristics*

Measurements of the frequency ω_i, and the amplitude δ_w of the waves were made for several reasons. Since the vertical velocity across the interface is continuous, the vertical velocity of the wave ($\sim \omega_i \delta_w$) is the same as the vertical turbulent velocity near the interface. As pointed out by Long (1978*b*), the r.m.s. amplitude of the waves is representative of the vertical size of the turbulent patches formed in the interfacial layer due to the wave breaking, and hence, its measurement is of importance in entrainment parameterizations (§4.2). Figure 8 depicts the variation of the r.m.s. frequency ω_i of the waves with the buoyancy frequency N indicating $\omega_i \simeq 1.4N$. The

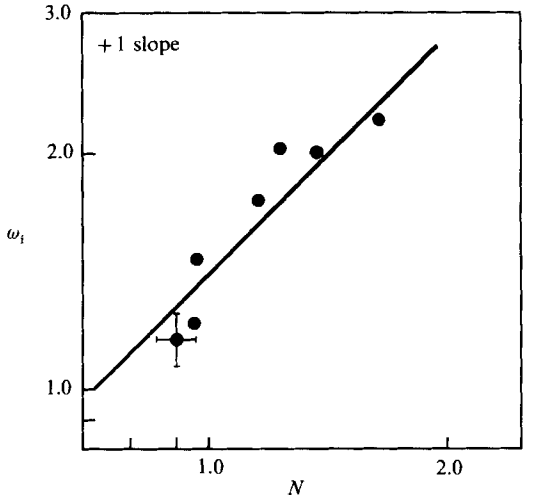

FIGURE 8. A log–log plot of interfacial wave frequencies (ω_i) *vs.* N. Both ω_i and N are in rad/s.

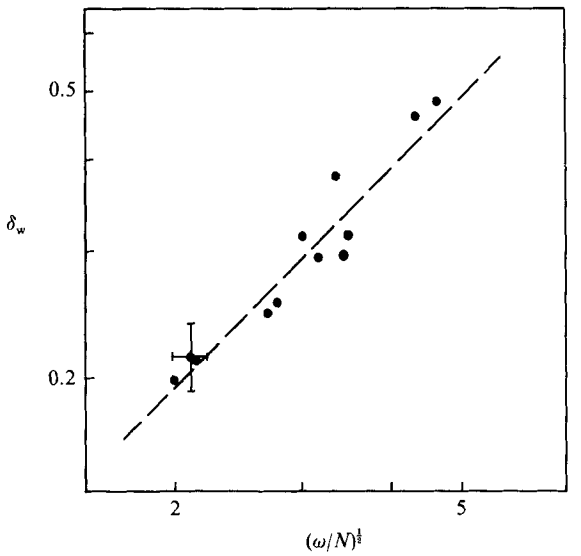

FIGURE 9. A log–log plot of interfacial wave amplitude (δ_w) *vs.* $(\omega/N)^{\frac{1}{2}}$. δ_w is in cm, ω and N are in rad/s.

measurements of the wave amplitude δ_w are presented in figure 9, and the data suggest that δ_w correlates well with the thickness of the patch $(K_1/N)^{\frac{1}{2}} \propto \omega/N)^{\frac{1}{2}}$ or $\delta_w \simeq 0.1 r_f$.

3.4. *Subsequent growth of the patch*

As noted earlier, the growth mechanisms of a turbulent patch at $t \gg t_f$ and $t < t_f$ are completely different and there is a transition between the two entrainment regimes at $r = r_f$. The results of measurements on the growth characteristics at $t \gg t_f$ are shown in figure 10 for the range $150 < Nt < 4000$. The mixed-layer thickness

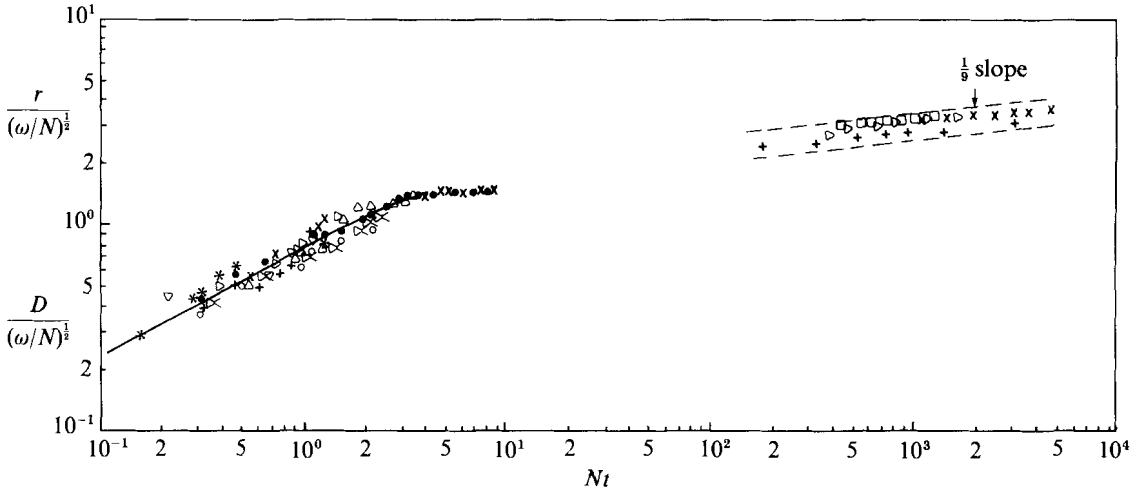

FIGURE 10. A log–log plot of $D/(\omega/N)^{\frac{1}{2}}$ *vs.* Nt at large Nt. Symbols represent ✕, $N = 1.49$ rad/s; $\omega = 14.5$ rad/s; □, 0.854, 12.5; ▷, 0.859, 12.5; +, 0.904, 12.5. Also included are the growth characteristics at small Nt values, i.e. $r/(\omega/N)^{\frac{1}{2}}$ *vs.* Nt. (D and r are in cm.)

D ($> r_f$), when normalized with $(\omega/N)^{\frac{1}{2}} \propto (K_1/N)^{\frac{1}{2}}$, collapses well with the non-dimensional time Nt, indicating a power law behaviour of the form

$$\frac{D}{(K_1/N)^{\frac{1}{2}}} \sim (Nt)^{\frac{1}{5}} \quad (t \gg t_f), \tag{4a}$$

or

$$D \sim K_1^{\frac{1}{2}} N^{-\frac{7}{18}} t^{\frac{1}{5}}. \tag{4b}$$

It is interesting that the observed power law given in (4) agrees well with the previous mixed-layer deepening experiments of Folse, Cox & Schexnayder (1981) and Fernando & Long (1985*a*) and the theory of mixing of Long (1978*b*). The growth characteristics for $t < t_f$ are included in figure 10 for convenience of comparison between the two entrainment regimes.

4. Theoretical considerations

4.1. *Growth characteristics of the patch*

To estimate the growth characteristics using a simple model, the following assumptions are made:

(*a*) The growth of the patch is one-dimensional (figure 1). Turbulence is horizontally homogeneous and nearly isotropic (Hopfinger & Toly 1976), with the exception that near the interface $w^2 = u^2 + v^2$ (Phillips 1955).

(*b*) The entrainment is caused by the engulfment of non-turbulent fluid by the energy-bearing eddies. Following Townsend (1976), this implies that

$$\frac{\partial r}{\partial t} = \beta w, \tag{5}$$

where β is constant. This mechanism becomes inoperative when the buoyancy forces limit the overturning motions of the eddies.

Constant	Value	Source
A	0.61	Hopfinger & Toly (1976)
k	2	Phillips (1955)
β	0.32	$A = k\beta$
B_1	0.15	Sreenivasan *et al.* (1980)
B_2	0.12	Fernando & Long (1985*a*, *b*)
C_1	1.18×10^{-2}	$C_1 = \beta B_1/2k$ or $\alpha = C_1/(1+C_2)$
C_2	1.0	Dickinson & Long (1978, 1983); present work
α	5.9×10^{-3}	present work

TABLE 1

(*c*) The buoyancy flux near the entrainment interface can be written as

$$(\overline{bw}) = B_1 bw, \tag{6}$$

where B_1 is a constant and b is the r.m.s. buoyancy fluctuation in the mixed region.

(*d*) The turbulent energy budget at the entrainment zone can be written as

$$\frac{\partial \frac{1}{2}q^2}{\partial t} = -(\overline{bw}) - \epsilon, \tag{7}$$

where $\frac{1}{2}q^2 = \frac{1}{2}(u^2+v^2+w^2)$ is the total turbulent kinetic energy and ϵ is the rate of turbulent kinetic-energy dissipation. The energy-flux divergence at the entrainment zone is assumed to be small although it is the major mechanism of energy transport in the bulk of the mixed layer (Hinze 1975).

If $q^2 = kw^2$, $k = 2$, and use is made of the well-known relation $\epsilon = Aw^3/r$, where A is a constant, and the experimental result $r = 2b/N^2$ (Van de Watering 1966), it is possible to combine (6) and (7) to obtain

$$\frac{\partial w^2}{\partial t} = -\frac{B_1}{k}N^2 rw - \frac{2A}{k}\frac{w^3}{r}. \tag{8}$$

The introduction of the non-dimensional variables $t_n = Nt$ and $r_n = r/r_*$ where r_* is a scaling length, and using (5), leads to

$$\frac{\partial^2 r_n}{\partial t_n^2} = -C_1 r_n - \frac{C_2}{r_n}\left(\frac{\partial r_n}{\partial t_n}\right)^2,$$

where

$$C_1 = \frac{\beta B_1}{2k}, \quad C_2 = \frac{A}{k\beta}. \tag{9}$$

The value of C_2 can be obtained by considering the mixed-layer growth in homogeneous fluids (i.e. $C_1 = 0$). The resulting equation has solutions of the form $r \sim t^m$ where $m(m-1) = -C_2 m^2$. Both previous (Dickinson & Long 1978, 1983) and present experiments, as well as theory (Long 1978*a*), suggest that the grid-generated mixed layer in a homogeneous fluid propagates as $r \propto t^{\frac{1}{2}}$, and hence $C_2 = 1$ and $A = k\beta$. For convenience, the estimated values of the relevant constants are listed in table 1. The solution of (9) can be written as

$$r_n^2 = \sin(2\alpha^{\frac{1}{2}} t_n), \tag{10a}$$

or in dimensional form, by evaluating the scaling length r_* in terms of the size of the patch† at $Nt = 1$, r_0,

$$r^2 = \frac{r_0^2}{\sin 2\alpha^{\frac{1}{2}}} \sin (2\alpha^{\frac{1}{2}} Nt), \tag{10b}$$

where $\alpha = C_1/(1+C_2) = \frac{1}{2}C_1$ needs to be evaluated from experimental evidence. The solid line in figure 4, up to $Nt \simeq 4$, is drawn corresponding to (10*b*), and has the form $r^2 \simeq 3.80(\omega/N) \sin 0.154\, Nt$, indicating $\alpha = 5.9 \times 10^{-3}$ and $r_0 = 0.76(\omega/N)^{\frac{1}{2}}$. The following points are worth noting:

(i) The smallness of the value of C_1, calculated using the measured α (table 1), indicates that during the initial growth of the patch, the second term of (9) is unimportant, as are buoyancy effects. For $\alpha^{\frac{1}{2}} \ll 1$, (10*b*) can be approximated by

$$r^2 \simeq \left[\frac{2\alpha^{\frac{1}{2}} N r_0^2}{\sin 2\alpha^{\frac{1}{2}}}\right] t, \tag{11}$$

which is the same as the power law behaviour observed in the grid-induced mixed-layer deepening experiments performed in homogeneous fluids by Dickinson & Long (1978, 1983). They showed that $r = (Kt)^{\frac{1}{2}}$, where K is proportional to K_1. In view of the result $r_0 = 0.76(\omega/N)^{\frac{1}{2}}$, it is easy to obtain $K \simeq 0.58\, \omega$.

To substantiate the claim that initial growth in the presence of stratification is similar to that of homogeneous fluids, several turbulent-layer propagation experiments were performed in homogeneous water (§2) and K was calculated by fitting the data to the expression $r = (Kt)^{\frac{1}{2}}$. Figure 11 shows the K values obtained from the front-propagation experiments in homogeneous fluids together with those calculated using (11) for the experiments presented in figure 4. The agreement seems to be satisfactory. Although only two values of K corresponding to (11) are shown, each of them represents the average of about five experiments performed at constant ω and variable N. Also, the results provided further evidence for the postulate $K_1 \sim K \propto \omega$.

(ii) As is evident from figure 4, beyond $Nt \simeq 4$, the growth behaviour does not follow (10). Instead, the mixed layer assumes an approximately constant vertical thickness $r_f \simeq 1.47(\omega/N)^{\frac{1}{2}}$. This observation can be explained on the basis of the limiting vertical lengthscale of the stratified turbulence. According to Long (1978*b*), the maximum (limiting) vertical size to which a turbulent patch in a stratified fluid can grow is determined by a balance between the vertical kinetic and potential energies of the mixed-layer eddies, viz.

$$w_f^2 = B_2 N^2 r_f^2, \tag{12}$$

where B_2 is a constant. For the present case, the limiting size of the patch can be evaluated using (5), (10) and (12) as

$$\frac{r_f}{r_*} = \frac{r_f}{r_0 \sin^{-\frac{1}{2}}(2\alpha^{\frac{1}{2}})} = \left[\frac{\alpha}{\alpha + B_2 \beta^2}\right]^{\frac{1}{4}}. \tag{13}$$

Substituting for α, B_2 and β (table 1), and using $r_0 = 0.76(\omega/N)^{\frac{1}{2}}$, the result is $r_f = 1.47(\omega/N)^{\frac{1}{2}}$, which is in excellent agreement with the experimental observations.

† Although the scaling length r_* in (10*a*) needs to be evaluated using boundary conditions, the fact that $r = 0$ at $t = 0$, makes r_* indeterminate. Hence the size of the patch at $Nt = 1$, r_0 is used as the scaling length.

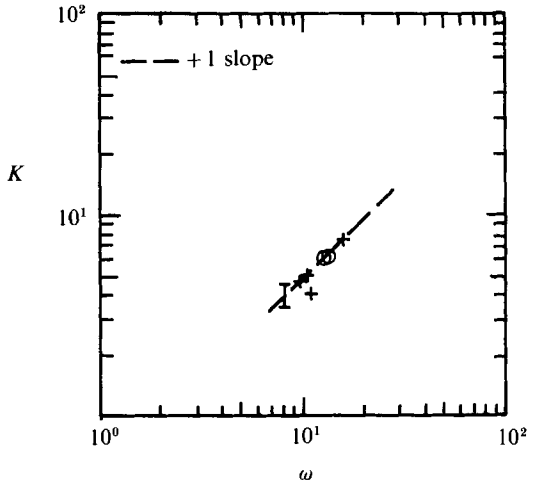

FIGURE 11. Variation of K (+, evaluated by the measurements of the turbulent layer propagation in a homogeneous fluid; ○, using (11)) with the frequency of grid oscillations (ω). K_1 is in cm^2/s and ω is in rad/s.

Further, the non-dimensional time taken to grow to this size $(t_n)_f$ can be calculated from (10) as

$$(t_n)_f = \frac{1}{2\alpha^{\frac{1}{2}}} \sin^{-1}(r_f/r_*)^2 \simeq 3.95, \tag{14}$$

which is also in agreement with the results of figure 4.

The observation that the mixed region grows to its limiting value at $Nt \simeq 4$ is worth comment. A change in the characteristics of stratified turbulence at $Nt = 3.5$–4.5 has been previously noticed by Dillon (1982). Dillon pointed out two cases, the collapse of a grid-generated wake at $Nt \simeq 4$ (Lange 1982) and the Nt values necessary for the turbulent lengthscales to grow to their maximum values during the decay of stratified turbulence (Stillinger *et al.* 1983). The grid-mixing experiments of Thorpe (1982), Ozmidov and Thorpe lengthscale measurements of Itsweire (1984), the decaying-turbulence measurements of Dickey & Mellor (1980) and the wake-collapse studies of Monroe & Mei (1968) are additional examples in which a distinct change in turbulence characteristics can be observed at $Nt \simeq 3.5$–4.5. Perhaps such a change in behaviour may be attributed to the inhibition of the evolution of turbulent patches at $Nt \simeq 4.0$.

Finally it is interesting to point out that the limiting patch size, given in (12), has the same form as the lengthscale $(\epsilon/N^3)^{\frac{1}{2}}$ proposed by Ozmidov (1965) for stratified turbulence. It is easily shown that (12) leads to

$$r_f = A^{-\frac{1}{2}} B_2^{-\frac{3}{4}} (\epsilon_f/N^3)^{\frac{1}{2}} \simeq 6.0(\epsilon_f/N^3)^{\frac{1}{2}}.$$

4.2. *Characteristics of the internal waves*

In previous sections, it was pointed out that the formation of an interfacial layer occurs when the mixed region grows to its limiting thickness r_f. Beyond r_f, the eddies of the size of the integral lengthscale of turbulence are not energetic enough to entrain the non-turbulent fluid by overturning motions, thus invalidating assumption (*b*) of the model presented in §4.1. Long (1978*b*) argued that, under such

circumstances, the eddies tend to flatten at the density interface, thus transferring their vertical kinetic energy to the horizontal components by a process similar to that which occurs during the distortion of homogeneous turbulence by a rigid boundary. Recent measurements have clearly indicated support for this postulation (Hannoun, Fernando & List 1988).

Long (1978*b*) and Carruthers & Hunt (1986) have theoretically analysed the distribution of turbulent velocity near a density interface. Both of these analyses take into consideration the distortion of eddies near a density interface and the excitation of internal waves due to the pressure fluctuations induced by the turbulence. However, in evaluating the vertical velocities near the interface, Long (1978*b*) considered the velocity field associated with the nonlinear mixing events occurring due to intermittent wave-breaking at the interface whereas Carruthers & Hunt (1986) performed a linear analysis which involves matching of the turbulence and wave motions at the interface. Further, Long (1978*b*) assumed that the wave motions are trapped within a layer adjacent to the interface (e.g. figure 3) while Carruthers & Hunt (1986) considered the possibility of internal wave radiation to the infinite extent of the stratified layer. Long's (1978*b*) analysis shows that the vertical velocity of the distorted eddies near the interface should be given by $w_i^2 \sim u_f^2(u_f/Nr_f) \sim (K_1 N)^{\frac{1}{2}}$, where u_f is the r.m.s. horizontal velocity at the location of the density interface prior to the distortion of turbulence by the density interface. Since the wave amplitudes (and hence the vertical size of the patches formed due to their breaking) should be governed by an expression of the form of (12), the r.m.s. wave amplitude may be evaluated, using $w_i^2 \sim N^2\delta_w^2$, as

$$\delta_w \sim (K_1/N)^{\frac{1}{2}} \sim (\omega/N)^{\frac{1}{2}}. \tag{15}$$

Also, the frequency of the waves can be written as,

$$\omega_i \sim w_i/N \sim N. \tag{16}$$

The analysis of Carruthers & Hunt (1986) suggests a different expression for the interfacial velocity, i.e. $w_i^2 \sim u_f^2(u_f/Nr_f)^{\frac{2}{3}}$. Nevertheless, substitution of the values for u_f and r_f gives $w_i \sim (K_1 N)^{\frac{1}{2}}$, and hence, for δ_w and ω_i, the same expressions as (15) and (16). These predictions are in agreement with the observations discussed in §3.3

4.3. *Subsequent growth of the patch*

As discussed in §3.4, the growth at $t \gg t_f$ takes place very slowly and the coalescence of mixed patches formed at the interface by the breaking waves with the rest of the mixed layer seems to be the cause for this growth. It it is assumed that the rate of change of potential energy (per unit horizontal area) of the system†, $\mathrm{d}\lambda/\mathrm{d}t$, i.e.

$$\frac{\mathrm{d}\lambda}{\mathrm{d}t} = \rho_0 N^2 D^2 \frac{\mathrm{d}D}{\mathrm{d}t}, \tag{17}$$

is proportional to the vertical energy flux $\rho_0 w_i^3$ available at the interface, then it is easily shown that the entrainment law should take the form

$$\frac{D}{(K_1/N)^{\frac{1}{2}}} \sim (Nt)^{\frac{1}{9}}, \tag{18}$$

† Which is the same as the horizontally averaged buoyancy flux integrated over the mixed layer.

if $w_i^2 \sim u^2(u/ND)$, according to Long (1978*b*), and

$$\frac{D}{(K_1/N)^{\frac{1}{2}}} \sim (Nt)^{\frac{1}{8}}, \tag{19}$$

if $w_i^2 \sim u^2(u/ND)^{\frac{2}{3}}$, according to Carruthers & Hunt (1986). Although the general trend of the present data follows (18), some individual runs show a behaviour closer to (19). Due to the closeness of the exponents of (18) and (19), it is difficult to assert from figure 10 which exponent is more appropriate, but several more detailed experiments, devoted to the determination of the entrainment law, can be found in the literature (Folse *et al.* 1981; E & Hopfinger 1986). Finally, it is interesting to note that (18) is equivalent to an entrainment law of the form $E \sim Ri^{-\frac{7}{4}}$, whereas (19) leads to $E \sim Ri^{-\frac{3}{2}}$, where E is the entrainment coefficient $u_e/(K_1/D)$, u_e is the entrainment velocity $\mathrm{d}D/\mathrm{d}t$ and $Ri = N^2 D^4/K_1^2$ is the overall Richardson number.

5. Discussion

The principal findings of the study described above are:

(i) When a turbulent region is generated in a linearly-stratified fluid, the initial growth of the mixed region is unaffected by the stratification, but as it grows to a certain vertical size, the buoyancy forces becomes important and suppress the vertical growth.

(ii) The inhibition of the growth occurs when the vertical size of the turbulent region becomes $r_f \sim (K_1/N)^{\frac{1}{2}}$. Scaling arguments suggest that this lengthscale can be interpreted as $r_f \sim w_f/N$ or $r_f \sim (\epsilon_f/N^3)^{\frac{1}{2}}$, where the turbulent quantities are evaluated prior to the distortion of turbulence by the density interface.

(iii) The resent experiments support the notion that the initial growth occurs by the engulfment of the non-turbulent fluid by the energy-bearing eddies at the entrainment interface. When the vertical kinetic and potential energies (or equivalently, the buoyancy and vertical inertia forces) of the eddies are of the same order this mechanism becomes inoperative. The entrainment process virtually stops and a well-defined density interfacial layer, which surrounds the mixed region, forms.

(iv) Internal waves are excited at the interfacial layer by the mixed-layer turbulence. Assuming that the amplitude of the waves are determined by a balance between the kinetic energy of the eddies and the potential energy fluctuations due to distortions, predictions were made for the frequencies and the amplitudes of these waves, and were compared with the experimental results.

(v) If the turbulent energy source is continuously maintained, the patch can grow very slowly beyond r_f. The observations reveal that this growth occurs by the merging of turbulent (mixed) patches, formed due to interfacial wave breaking, with the rest of the mixed layer.

Some of the above findings have applications to practical flow situations. For instance, as pointed out by Pao (1973), a knowledge of the conditions for the formation of an interfacial layer is required to detect clear-air-turbulence (CAT) regions using radar back-scatter signals; weak turbulent regions surrounded by a density interfacial layer can yield strong radar echoes whereas strong CAT regions without the density interfacial layer can yield weak signals. It is well known that the turbulence in the oceanic thermocline is confined to intermittently occurring turbulent patches. These patches are created by spasmodic turbulence-generating

events such as the breaking of internal waves. While the patches grow, the turbulence decay and the vertical size of these patches are limited by the criterion given by (12). Lateral gravitational spreading of the mixed fluid is an additional feature of these patches. Of course, such complicated features found in natural flows are not simulated in the present experiments; nevertheless, the observations verify that the vertical growth of these patches is drastically affected by buoyancy forces, once they grow to a certain size. As estimated in §4.1, the limiting vertical size of these patches is given by $r_f \simeq 6.0\ (\epsilon_f/N^3)^{\frac{1}{2}}$, implying that for characteristic ϵ_f (3×10^{-5} to 5×10^{-3} cm^2/s^3) and $N(\sim 1.5 \times 10^{-2}$ s^{-1}) values of the ocean (Osborn 1980), the vertical size of the microstructure patches may vary from several centimetres to a few metres.

The demonstration of the existence of a transition between two entrainment regimes at the limiting patch size is another significant feature of the present experiments. When $r < r_f$, the large-scale eddies are directly involved in the entrainment process, leading to an entrainment law of the form $E \sim 1$, whereas when $r > r_f$, local instabilities of the interfacial layer are responsible for mixing and the entrainment law takes the form $E \sim Ri^{-\frac{7}{4}}$ or $Ri^{-\frac{3}{2}}$.

The experiments reported here were performed when the author was a research fellow at CalTech. The author wishes to thank Professor E. John List for his encouragement and hospitality and Professors D. F. Jankowski, G. P. Neitzel and G. Oth for their help in numerous ways. The referees provided valuable comments that led to a considerable improvement of this paper. The financial support of the National Science Foundation, Grant nos. CEE 7272A1, MSM 8504909 and the Office of Naval Research Contract no. N 00014-87-K-0423 is gratefully acknowledged.

REFERENCES

CALDWELL, W. 1983 Oceanic turbulence: Big bangs or continuous creation. *J. Geophys. Res.* **88**, 8543.

CARRUTHERS, D. J. & HUNT, J. C. R. 1986 Velocity fluctuations near an interface between a turbulent region and a stably stratified layer. *J. Fluid Mech.* **165**, 475.

CRAWFORD, W. 1982 Pacific equatorial turbulence. *J. Phys. Ocean* **12**, 1136.

DICKEY, T. D. & MELLOR, G. L. 1980 Decaying turbulence in neutral and stratified fluids. *J. Fluid Mech.* **99**, 13.

DICKINSON, S. C. & LONG, R. R. 1978 Laboratory study of the growth of a turbulent layer of fluid. *Phys. Fluids* **21**, 1698.

DICKINSON, S. C. & LONG, R. R. 1983 Oscillating grid turbulence including the effects of rotation. *J. Fluid Mech.* **126**, 315.

DILLON, T. M. 1982 Vertical overturns; a comparison of Thorpe and Ozmidov length-scales. *J. Geophys. Res.* **87**, 9601.

DOUGHERTY, J. P. 1961 The anisotropy of turbulence at meteor level. *J. Atmos. Terr. Phys.* **21**, 210.

E, X. & HOPFINGER, E. J. 1986 On mixing across an interface in a stably stratified fluid. *J. Fluid Mech.* **166**, 227.

FERNANDO, H. J. S. & LONG, R. R. 1985*a* The deepening of a mixed layer in a linearly stratified fluid. *Phys. Fluids* **28**, 2999.

FERNANDO, H. J. S. & LONG, R. S. 1985*b* On the nature of the entrainment interface of a two-layer fluid subjected to zero-mean-shear turbulence. *J. Fluid Mech.* **151**, 21.

FOLSE, R. F., COX, R. P. & SCHEXNAYDER, K. R. 1981 Measurements of the growth of a turbulently mixed layer in a linearly stratified fluid. *Phys. Fluids* **24**, 396.

GIBSON, C. H. 1981 Buoyancy effects in turbulent mixing: sampling turbulence in stratified ocean. *AIAA J.* **19**, 1394.

GIBSON, C. H. 1986 Internal waves, fossil turbulence, and composite ocean microstructure spectra. *J. Fluid Mech.* **168**, 89.

HANNOUN, I. A., FERNANDO, H. J. S. & LIST, E. J. 1988 Turbulence structure near a sharp density interface. *J. Fluid Mech.* **189**, 189.

HINZE, J. O. 1975 *Turbulence*, 2nd edn. McGraw-Hill.

HOPFINGER, E. J. & TOLY, J.-A. 1976 Spatially decaying turbulence and its relation to mixing across density interfaces. *J. Fluid Mech.* **78**, 155.

ITSWEIRE, E. C. 1984 Measurements of vertical overturns in a stably stratified turbulent flow. *Phys. Fluids* **27**, 764.

LANGE, R. E. 1982 An experimental study of turbulence behind towed biplanar grids in salt-stratified fluids. *J. Geophys. Res.* **12**, 1506.

LONG, R. R. 1978*a* Theory of turbulence in a homogeneous fluid induced by an oscillating grid. *Phys. Fluids* **21**, 1887.

LONG, R. R. 1978*b* A theory of mixing in stably stratified fluids. *J. Fluid Mech.* **84**, 113.

LONG, R. R. 1986 Some aspects of the decay of turbulence. *Phys. Fluids* (submitted).

MCEWAN, A. D. 1983*a* Internal mixing in stratified fluids. *J. Fluid Mech.* **128**, 59.

MCEWAN, A. D. 1983*b* The kinematics of stratified mixing through internal wave breaking. *J. Fluid Mech.* **128**, 47.

MONROE, R. H. & MEI, C. C. 1968 The shape of two-dimensional turbulent wakes in density-stratified fluids. *MIT Hydrodyn. Lab. Rep. no.* 110.

OSBORN, T. 1980 Estimates of local rate of vertical diffusion from dissipation measurements. *J. Phys. Ocean* **10**, 83.

OSTER, G. & YAMAMOTO, M. 1963 Density gradient techniques. *Chem. Rev.* **63**, 257.

OZMIDOV, R. V. 1965 On the turbulent exchange in a stably stratified ocean. *Bull. Acad. Sci. USSR Atmos. Ocean. Phys.* **1**, 493–497.

PAO, Y.-H. 1973 Measurements of internal waves and turbulence in two-dimensional stratified shear flows. *Boundary-Layer Met.* **5**, 177.

PHILLIPS, O. M. 1955 The irrotational motion outside a free turbulent boundary. *Proc. Camb. Phil. Soc.* **51**, 220.

SREENIVASAN, K. R., TAVOULARIS, T., HENRY, R. & CORRSIN, S. 1980 Temperature fluctuations and scales in grid generated turbulence. *J. Fluid Mech.* **100**, 597.

STILLINGER, D. C., HELLEND, K. N. & VAN ATTA, C. W. 1983 Experiments on the transition of homogeneous turbulence to internal waves in a stratified fluid. *J. Fluid Mech.* **131**, 91.

THORPE, S. A. 1982 On the layers produced by rapidly oscillating a vertical grid in a uniformly stratified fluid. *J. Fluid Mech.* **124**, 391.

TOWNSEND, A. 1976 *Structure of Turbulent Shear Flow*. Cambridge University Press.

VAN DE WATERING, W. P. M. 1966 The growth of a turbulent wake in a density stratified fluid. *Tech. Rep.* 231–12, Hydronautics, Inc.

WYATT, L. R. 1978 The entrainment interface in a stratified fluid. *J. Fluid Mech.* **86**, 293.